Research & Reviews: Journal of Material Sciences e-ISSN: 2321-6212

Comparison of Two Mechanical Alloying Synthesis of WMoTaNbCr and WMoTaNbTi

Ignacio Orellana Araya, Claudio Aguilar Ramírez*

Department of Metallurgical and Materials Engineering, Universidad Técnica Federico Santa María, Valparaíso, Chile

Research Article

Received: 20-May-2022, Manuscript No. JOMS-22-64350; **Editor assigned:** 23-May-2022, PreQC No. JOMS-22-64350 (PQ); **Reviewed:** 06-Jun-2022, QC No. JOMS -22-64350; **Revised:** 13-Jun-2022, Manuscript No. JOMS -22-64350 (R); **Published:** 20-Jun-2022, DOI: 10.4172/2321-6212.10.6.002.

***For Correspondence:**
Claudio Aguilar Ramírez,
Department of Metallurgical and Materials Engineering, Universidad Técnica Federico Santa María,
Valparaíso, Chile

E-mail: b.ankara@yandex.com

Keywords: Refractory high entropy alloy; Rietveld refinement; Mechanical alloying; Grinding media contamination

ABSTRACT

Mechanical alloying is a route that prevents the common dendrite structure with segregation and avoids the problems related to the grain growth present in arc melting, besides allowing the alloying of elements with a high melting point at room temperature and limited solubility. In this study, the phase evolution of two refractory high entropy alloys was developed, WTaMoNbCr and WTaMoNbTi, in two different conditions of mechanical alloy: with detentions intervals and continuous mechanical alloying. The first one produces the face-centered cubic single solid solution WTaMoNbCr and WTaMoNbTi with lattice parameters 0.4313 and 0.4305 nm, respectively. The second mechanical alloying produced a widening of the lattice parameter to 0.4319 and 0.4325 nm of the WTaMoNbCr and WTaMoNbTi, respectively, due to the high contamination related to the process.

INTRODUCTION

Refractory alloys are commonly required in energy, aircraft, and aerospace industries, where turbine blades, discs, jet engines, structural components, and coating, are some examples of their application. Superalloys such as nickel-base, cobalt-base, and iron-base were developed as materials for elevated temperatures thanks to their outstanding strength at high temperatures and corrosion resistance. Despite their properties, the components show service-induced degradation which can be attributed to a metallurgical or mechanical origin, for instance for a gas turbine engine component more than 50% of failures are due to fatigue [1-5]. For this reason, material science continuously is developing and improving its strategy to enhance the applicability of refractory materials. That is how high entropy alloys play a powerful role in the new design of refractory material. Refractory High Entropy Alloys (RHEA) are considered promising alternatives to elevated temperature applications. RHEA as NbMoTaW and VNbMoTaW were studied by vacuum arc melting showing a single-phase-Body-Centered Cubic (BCC) crystal structure and making a comparison with Inconel 718 and Haynes 230, both RHEA demonstrate a superior yield strength above 800 °C (typical operation temperature of superalloys), with a strong resistance to high temperature softening [6]. Hang et al. studied the effect of the Ti in the alloys NbMoTaW and VNbMoTaW, proving the enhanced strength and ductility, where the room temperature yield strength of TiNbMoTaW and TiVNbTaMoW is 1343 MPa and 1515 MPa, respectively, with a compressive plastic strain above 10%, meanwhile the room temperature yield strength of NbMoTaW and VNbMoTaW is 1058 MPa and 1246 MPa, with a low ductility of about 2.0% and 1.5%, respectively [7].

Typically, RHEAs are produced by arc melting temperature, but several processing routes have been used to prepare these alloys, such as sputtering [8], splat quenching [9], and mechanical alloying. Mechanical alloying (MA) is a route that prevents the common dendrite structure with some micro-segregation [10-14], formation of intermetallic, and avoiding the problems related to the grain growth in the melting process [15], besides that allow the formation of metastable phases and supertasured solutions [16]. A few reviews attempt to provide a comprehensive and critical analysis of the potentials and limitations of mechanically alloyed High Entropy Alloys (HEAs) [17,18]. Additionally, for some applications the arc melting/casting routes are unsuitable for industrial manufacturing due to the limitations in shape and size of final products, and the disadvantages of diseconomy [19]. For instance, Kang et al. proved that the WTaMoNbV alloys consolidated by SPS at 1500 °C had a noticeable increase of yield strength of 2612 MPa and 8.8% of strain in a room-temperature compression test, while the arc melting alloy showed a yield strength of 1246 MPa and a plastic strain of 1.7%. The difference between the mechanical properties was attributed to the small grain size of the SPS specimen of 5.30 μm, the solid solution hardening by C and O related to the sintering process, and the presence of Ta_2VO_6 precipitated [20], similar properties have been found in the alloys TaTiZrNbAl with a high yield strength of 1740 MPa with considerable compressive plasticity of 12% at room temperature [21], and NbTaTiV with a yield strength of 1370 MPa and a fracture strain of 23% at room temperature [22].

This research focused on two RHEA WMoTaNbCr and WMoTaNbTi systems, fabricated by the conventional powder metallurgical process. Two strategies of mechanical alloying are investigated: the first one considers the detention of the planetary ball mill, and the second one consists of a continuous operation of the ball mill. The objective of the current study establishes a powder metallurgical route, characterize its phases and microstructure.

MATERIALS AND METHODS

The formation of the alloys WMoTaNbCr and WMoTaNbTi was carried out with an equimolar composition. W, Mo, Ta, Nb, Cr, and Ti powder with a purity of 99.9% were used in this study, with a particle size smaller than 75 μm. The raw powders were placed in Yttria-stabilized zirconia vials in equiatomic ratio filled by balls of the same material (ratio 1:1 of 5 and 10 mm in diameter). The mechanical alloying process was conducted with 2 wt% stearic acids as a Process Control Agent (PCA) in a high-energy planetary ball mill Retsh PM400 at 250 rpm, with a ball-to-powder ratio of 10:1 and in an ultra-high purity argon atmosphere to prevent oxidation. A pre-milling was carried out for 2 h with a few grams of elements powder to coat the grinding media. Two strategies of mechanical alloying are carried out: (i) to analyze the milling kinetics of each alloy, powder samples (0.1 g) were sampled after 5, 10, 30, 50, and 100 h of milling. These procedures were carried out inside a glove box to prevent oxidation of the powders; (ii) in the second mechanical alloying the powders were milled for continuous 100 h with no detention times.

The crystal structure of the powders samples was analyzed by X-ray diffraction, XRD STOESTADI MP using Cu Kα radiation, and the Rietveld Refinement is made using the MAUD software. The shape and elements distribution of the elements in the powder was analyzed by field-emission scanning electron microscopy QUANTA FEG 250 and Energy-Dispersive X- Ray Spectroscopy (EDS).

RESULTS AND DISCUSSION

Phase evolution during MA of the first mechanical alloying

The XRD patterns of the alloys prepared at each ball milling duration are presented in Figure 1. The initial diffraction peaks of all the pure elements can be observed in the initial blending powders denoted as 0 h. For the WMoTaNbCr alloy, the 5 h milled powder show that Ta and Nb form a BCC solid solution which is expectable due to the similar atomic radii (0.143 nm [23]), and appear the first principle (111) diffraction peak of an FCC phase, at 10 h milled powder the Cr start to enter in the solid solution, while Mo diffuses into the W structure (atomic radii of Mo and W are 0.136 nm and 0.137 nm, respectively), and remain only the (110) plane of the BCC phase. The FCC phase and W peaks co-exist at 30 h milled powder, besides peaks broadening due to the decreased of crystallite size related to the mechanical alloying are noticeable. It can be hypothesized that the solid solution sequence of the elements is related to the melting point, with low melting point elements being dissolved quickly, similarly reported in other work [24]. When the milling time reaches 100 h only the FCC phase can be found. A similar behavior shows the WMoTaNbTi alloy where Ta, Nb, and Ti form a BCC solid solution at 5 h milled time, with the presence of a (111) FCC plane diffraction and Mo diffusing into the W structure. At 10 h milled time, only the W peaks with the principle (111) FCC plane are present, until the milled time increase to 100 h where only the FCC phase exists.

The results of Rietveld refinement are shown in Table 1, indicating a nanocrystalline size and high micro-strain of the alloys, related to the high energy process, in agreement with the mechanical alloying of other RHEAs as shown the Table 2 in the major cases with a BCC crystal structure. The lattice parameter in Table 3 indicated a difference between the BCC phases obtained in other works and the FCC phase in the present work, although when the NbMoTaWVTi alloy is consolidated by SPS an FCC phase is observed with a lattice parameter of 0.4235 nm, similar to the lattice parameter of the FCC phase of this work [25].

Figure 1. XRD patterns of the milled powders with 0, 5, 30, 50 and 100 h: (a) WMoTaNbCr alloy; (b) WMoTaNbTi alloy. (Note: ○ Cr, ■ Nb, □ Mo, ▲ Ta, △W, ▽BCC, ⊗FCC)

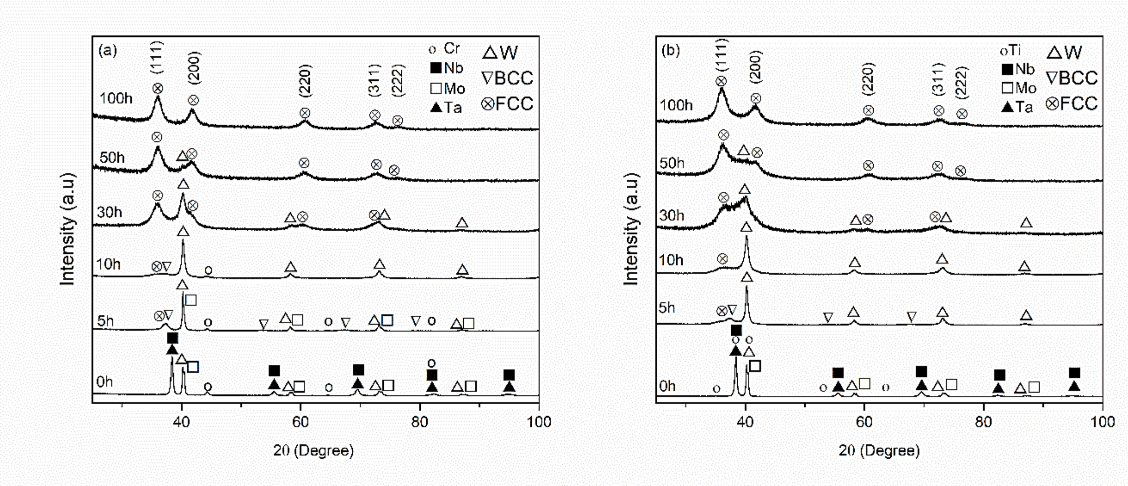

Table 1. Lattice parameter, crystallite size, and micro-strain of FCC solid solution at 100 h milled time, first mechanical alloying.

Alloy	Lattice Parameter, nm	Crystallite size, nm	Micro-strain, -
WMoTaNbCr	0.4313	44.77	0.0106
WMoTaNbTi	0.4305	4.06	0.0029

Table 2. Parameters of different HEAs processed through the MA technique.

HEA powders	Crystallite size, nm	Micro-strain, -	Phase	Ref.
NbMoWZrV	11	0.0058	BCC+FCC	[26]
NbMoTaW	11.8	0.0069	BCC	[27]
NbMoTaWV	66.1	0.0096	BCC	[28]
MoNbTaTiV	12.9	0.0089	BCC	[29]
WMoVCrTa	3.16	-	BCC	[30]

Table 3. Lattice parameter of different RHEAs processed through MA technique.

HEA alloy	Milling time, h	Lattice parameter, nm	Phase	Ref.
VNbMoTaW	30	0.3146	BCC	[31]
NbMoTaWVTi	20	0.3172	BCC	[25]
WNbMoTaV	6	0.3186	BCC	[20]
$TiNbTa_{0.5}ZrAl_{0.5}$	10	0.3355	BCC	[21]

Prediction of the crystal structure of a single-solid solution-phase based on the Hume-Rothery Rules [32] can be carried out using the VEC parameter which has the definition of the number of total electrons including the *d*-electrons accommodated in the valence band, defined mathematically

$$VEC = \sum_{i=1}^{n} c_i (VEC)_i$$

where c_i and $(VEC)_i$ are the VEC and the atomic percentage for the individual element i. Guo *et al*. determined that BCC phases occur at $VEC \leq 6.87$, FCC phases at $VEC \geq 8$, and a mixture of FCC and BCC at $6.87 \leq VEC \leq 8$ [33]. The calculation of the VEC parameter for WMoTaNbCr and WMoTaNbTi alloys are 5.6 and 5.2, respectively, predicting a BCC phase for both alloys. Generally, the refractory elements have VEC values minor than 6, for instance, Zr (4), Hf (4), and the elements listed in Table 4 producing RHEAs with VEC less than 6.86 stabilizing BCC phases as can be noticed in the comprehensive data compilation of Couzinié et al. [34]. Furthermore, WMoTaNbTi alloy produced by arc melting [35] and selective electron beam melting [36], with a single BCC phase support the theory. Thus, the 100 hours mechanical alloying carried out and presented in the Figure 1 suggest that the FCC phases for both alloys are metastable phase, which is expectable in this route process due to the high energy supplied to the powders, even being capable to produce high entropy glasses or amorphous alloys [37]. Despite of the FCC single solid solution, for both alloys a BCC phase transition can be observed at 5 h milling time disappearing rapidly at 10 h (for WMoTaNbCr alloy just remain de (110) peak at 10 h). As shown the Table 3 the RHEAs processed through MA produced a BCC single solid solution at milling time below 30 h, thus probably a 100 h mechanical alloying induced a high energy to the powders producing the formation of an FCC phase.

Table 4. VEC for elements [38].

Elements	VEC
W	6
Mo	6
Ta	5
Nb	5
Cr	6
Ti	4

The elemental mapping of the WMoTaNbCr alloy by FESEM presented in Figure 2 indicates a homogeneous distribution of the refractory elements with no segregation, as well as WMoTaNbTi in Figure 3. These results are in good agreement with the previous analysis, which evidences the solid solution of all refractory elements at 100 h mill time.

Figure 2. FESEM image and element distribution of the 100 h milled WMoTaNbCr powder.

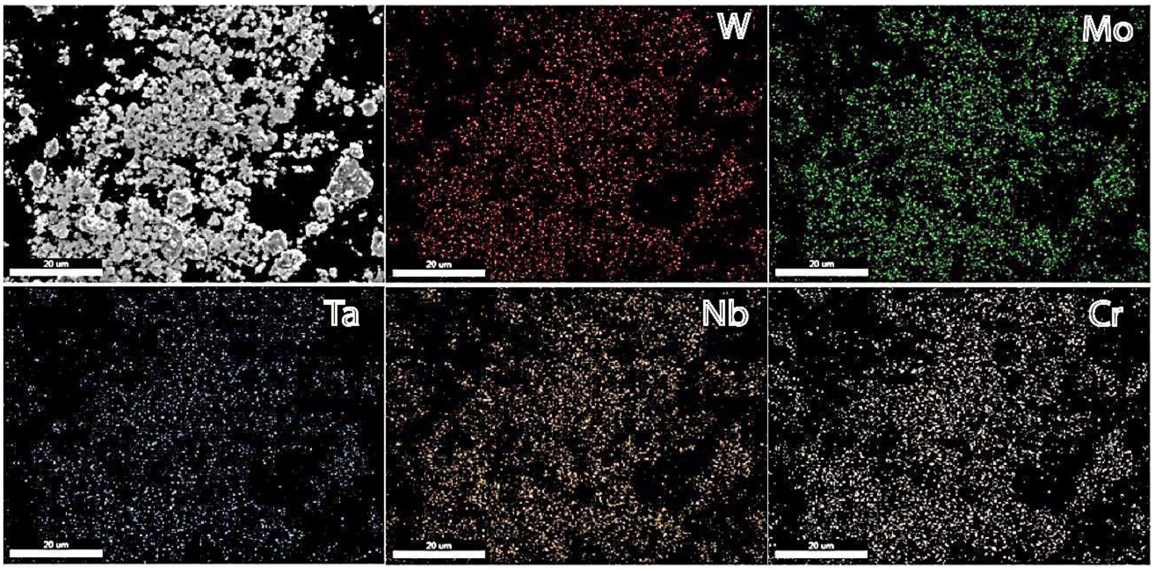

Figure 3. FESEM image and element distribution of the 100 h milled WMoTaNbTi powder.

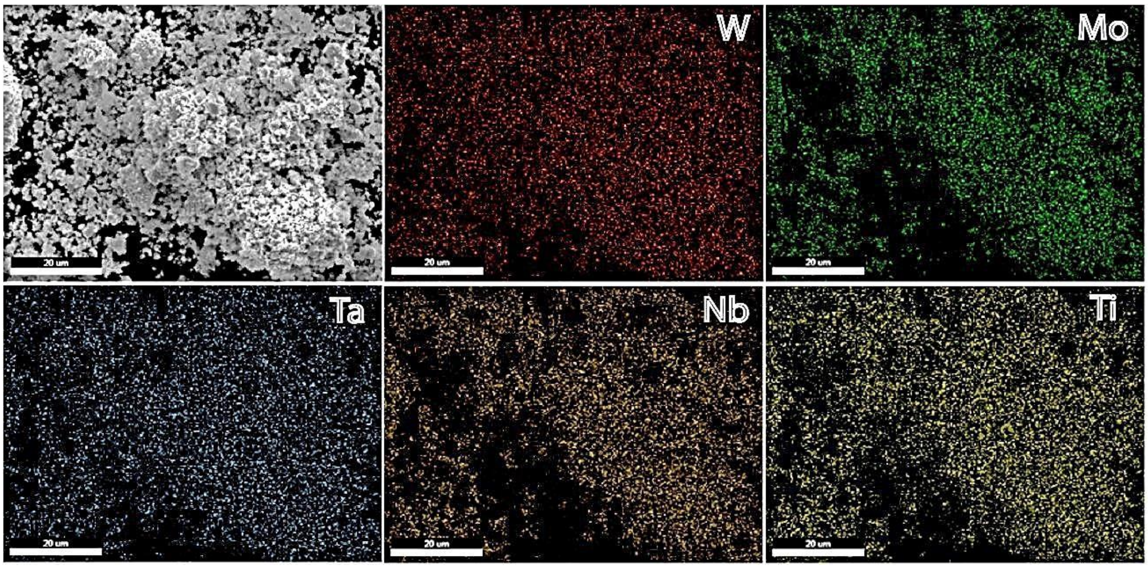

Phase evolution during MA of the second mechanical alloying

By contrast, Figure 4 illustrate the second set of powders, which were mechanically alloyed in the same condition, but with the difference that the milling time was 100 continuous hours, unlike the first milled powders which had detention times, where all the content of the vials were manipulated to take off the powders from the balls and the inners walls. When the second set of powders stop the MA process, the powders were deposited in the bottom of the vials a compacted, so it was necessary to pound the materials with a spoon. The effect of this phenomenon is observed in Figure 4. The effective milling time is located between 10 and 30 h of the first MA, with very high contamination of the grinding media, Yttria-stabilized zirconia. Besides, the W and FCC peaks are shifted to a minors angle, as demonstrated the Figure 5, revealing that the Zr diffuse in the W and FCC crystal structure. Furthermore, the atomic radius analysis supports the evidence, since the atomic radius of Zr is 0.162 nm, while the W radius atomic is 0.137 nm. With this in mind, it is possible that atoms of Zr could drop from the balls and walls of the vial and diffuse into the W structure, increasing the lattice parameter. A similar phenomenon occurs with the FCC phase. The previous statement is corroborated by taking into account the results of the Rietveld refinement in Table 5 when comparing the lattice parameter of the FCC high entropy alloy of Table 1 noticing an increase, and the same phenomenon occurs with the W structure when its regard that the Crystallographic Information File (CIF) used, consider the value 0.3164 nm (3.1648 Å).

Figure 4. XRD patterns of the 10 h and 30 h of the first mechanically milled powders and the 100 h of the second milled powders (denoted by 100 h*): (a) WMoTaNbCr alloy; (b) WMoTaNbTi alloy. (**Note:** ○ Cr, ⊗FCC, △W, ▽BCC, ◒ZrO_2-Y_2O_3)

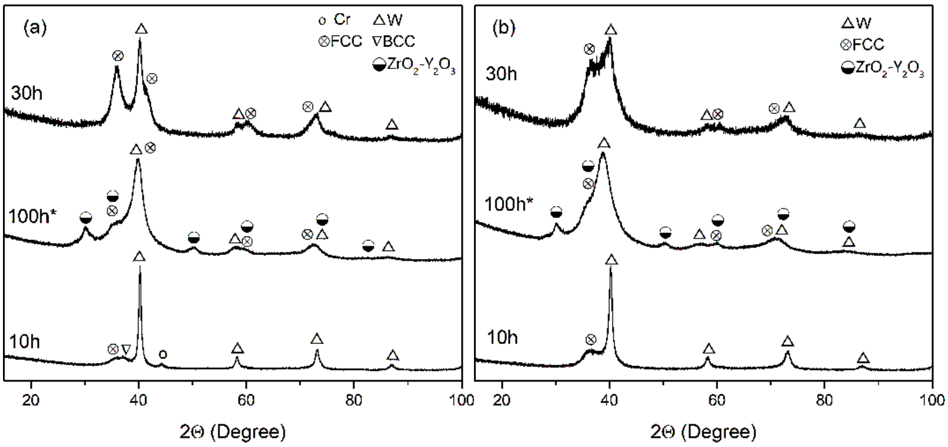

Figure 5. Detailed XRD patterns with a zoom between 30°-50°. Comparison of the first and second MA. (**Note:** ○ Cr, ⊗FCC, △W, ▽BCC, ◒ZrO_2-Y_2O_3)

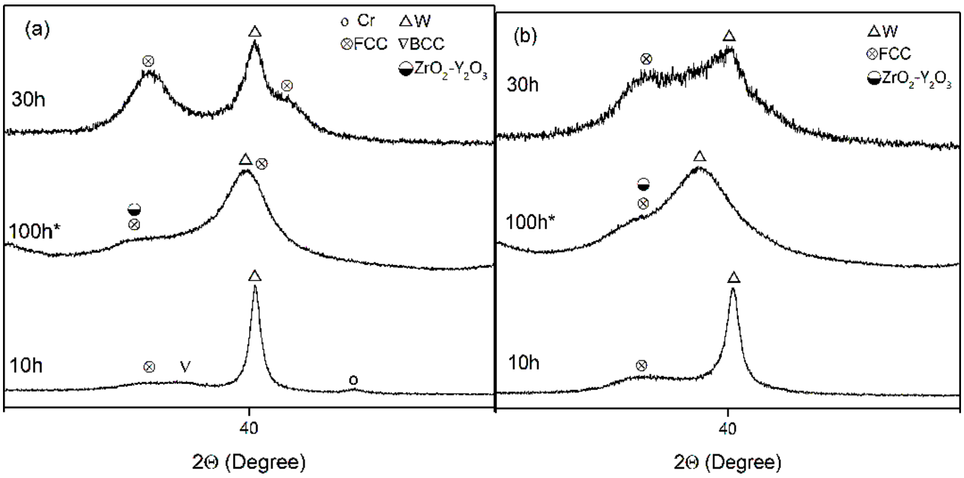

Table 5. Lattice parameter of FCC solid solution and W at 100 h milled time, second mechanical alloying.

Phases	Lattice Parameter, nm
FCC in WMoTaNbCr	0.4319
FCC in WMoTaNbTi	0.4325
W in WMoTaNbCr	0.3208
W in WMoTaNbTi	0.3268

The inhomogeneity of the elements in the powders is evident in Figure 6, for instance, for the WMoTaNbCr alloy there is a zone 1 rich in W, Mo, and Nb, and a zone 2 is rich in Cr and Ta. A similar situation is shown in Figure 7 with the WMoTaNbTi alloy where there is a clear segregation of the Mo, Nb, and Ti.

Figure 6. FESEM image and element distribution of the 100 h milled WMoTaNbCr powder compacted, 10000X.

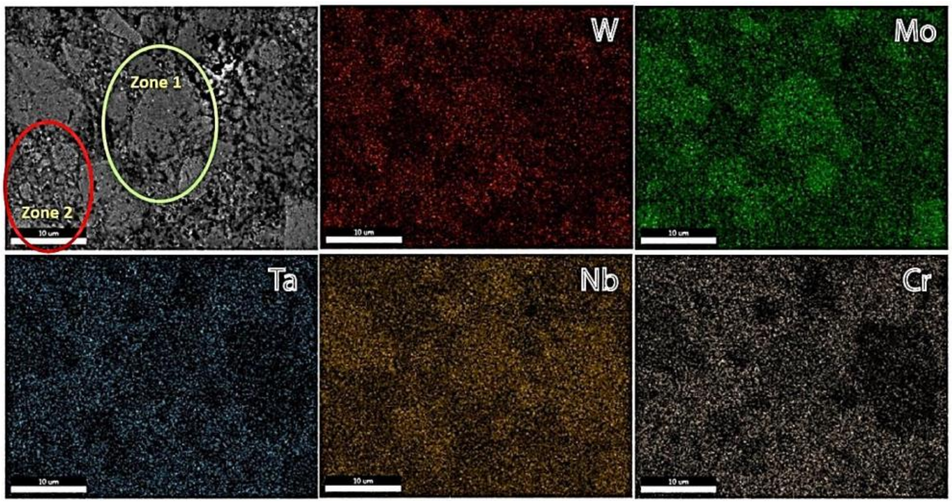

Figure 7. FESEM image and element distribution of the 100 h milled WMoTaNbTi powder compacted, 10000X.

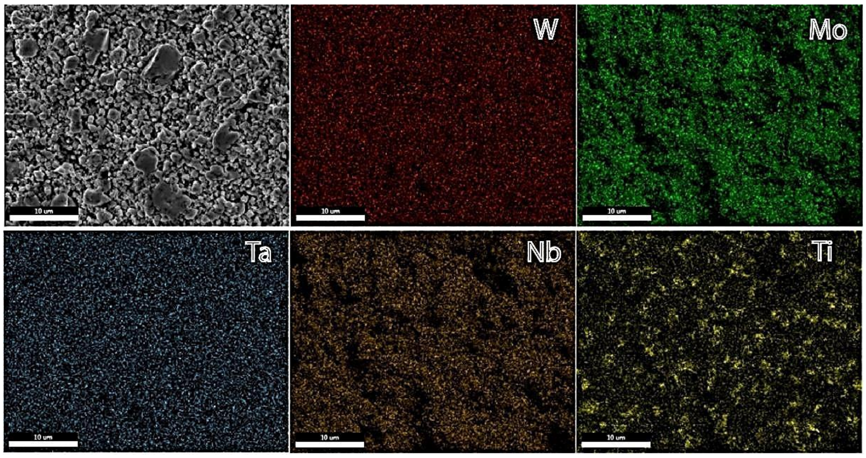

The presence of Zr is demonstrated by the mapping in Figure 8 and shows that the material of the grinding media drops and is alloyed. With the mapping of Figure 6 can be suggested that Zr and Nb form a solid solution. This analysis confirms the DRX results shown before (Figures 4 and 5). The contamination of the grinding media as a ceramic $((ZrO_2)0.89(Y_2O_3)0.11)0.901$ is quantified through Rietveld Refinement obtained for the alloy WMoTaNbCr and WMoTaNbTi, 20.4 wt% and 21.8 wt% of contamination, respectively. The last analysis is relevant because demonstrates that the contamination by grinding media is an important factor to keep in mind, for instance, it has been found that in 5 h milling time Zr could lead to the incorporation of about 6 wt.% as part of the powders [39], and the previous investigation has proven that agate (SiO_2) and zirconia grinding media, despite their inert nature at room temperature, can easily contaminate the powders and be mechanochemical reactive, while tungsten carbides (WC) grinding media show better behavior [40].

Figure 8. Zr mapping of the 100h milled powder compacted, 10000X: a) WMoTaNbCr; b) WMoTaNbTi.

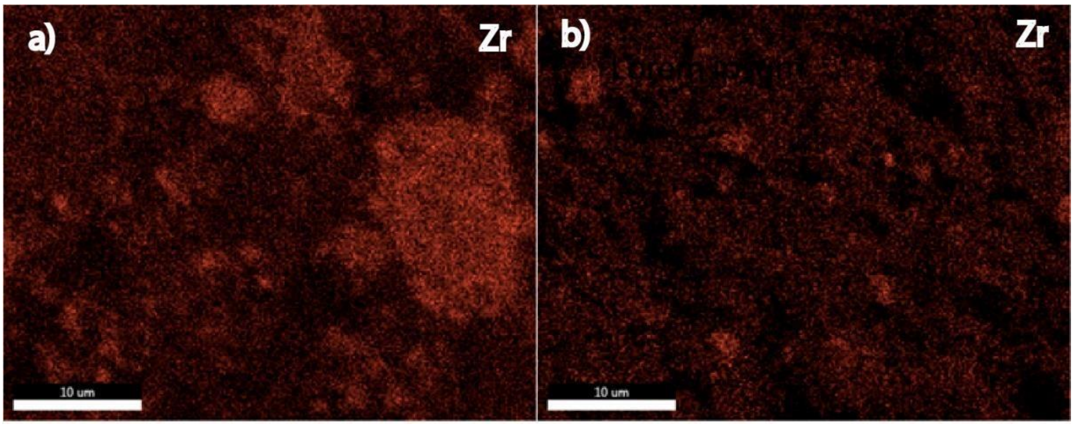

CONCLUSION

WTaMoNbCr and WTaMoNbTi refractory high entropy alloys were obtained by two different Mechanical Alloying (MA) conditions. The evolution of the phases in the first MA show at 100 h milling time the formation of a face-centered cubic with a lattice parameter of 0.4313 and 0.4305 nm for the nanocrystalline WTaMoNbCr and WTaMoNbTi alloy, respectively. In contrast, the second MA demonstrated that the effective milling time is between 10 and 30 h of the first MA, with important contamination of ZrO_2-$Y2O_3$ and the shift of the peaks to lower angles due to the incorporation of Zr atoms in the crystals, increasing the lattice parameters of the phases. The contamination was quantified by Rietveld Refinement for the WTaMoNbCr and WTaMoNbTi obtaining 20.4 wt% and 21.8 wt%, respectively. Finally, the route of mechanical alloy plays a fundamental role in the final results of the mechanical alloys, and the parameters of the process as the grinding media and detentions time must be chosen wisely.

ACKNOWLEDGMENT

The authors would like to thank the University Federico Santa María, especially the Research Powder Metallurgy laboratory, the support provided by FONDECYT grant no 1190797, and the "Piensa Minería" program of Codelco.

REFERENCES

1. Mishra RK, et al. Failure analysis of an un-cooled turbine blade in an aero gas turbine engine. Eng Fail Anal. 2016;79:836-844.
2. Poursaeidi E, et al. Failure analysis of a second stage blade in a gas turbine engine. Eng Fa Anal. 2008;15: 1111-1129.
3. Cowles BA. High cycle fatigue in aircraft gas turbines—an industry perspective. Inter Jou of Fract. 1989;80:147-163.
4. Mishra, et al. Failure of low-pressure turbine blades in military turbofan engines: causes and remedies. Jour of Fail Anal and Prev. 2016;16:622-628.
5. Čerňan J, et al. Damages of RD-33 Engine Gas Turbine and their Causes. Trans Res Pro. 2018;35:200-208.
6. Senkov ON, et al. Mechanical properties of $Nb_{25}Mo_{25}Ta_{25}W_{25}$ and $V_{20}Nb_{20}Mo_{20}Ta_{20}W_{20}$ refractory high entropy alloys. Intermetallics. 2011;19:698-706.
7. Han ZD, et al. Effect of Ti additions on mechanical properties of NbMoTaW and VNbMoTaW refractory high entropy alloys. Intermetall. 2017;84:153-157.
8. An Z, et al. Solid-solution CrCoCuFeNi high-entropy alloy thin films synthesized by sputter deposition. Mater Rese Lett. 2015;3:203-209.
9. Singh S, et al. Decomposition in multi-component AlCoCrCuFeNi high-entropy alloy. Acta Materialia. 2011;59:182-190.
10. Han Z, et al. Microstructure, phase stability and mechanical properties of Nb-Ni-Ti-Co-Zr and Nb-Ni-Ti-Co-Zr-Hf high entropy alloys. Prog in Natu Scie: Mate Inter. 2015;25:365-369.
11. Fu Z, et al. Effects of Co and sintering method on microstructure and mechanical behavior of a high-entropy $Al_{0.6}NiFeCrCo$ alloy prepared by powder metallurgy. Jour of Allo and Comp. 2015;646:175-182.
12. Guo NN, et al. Microstructure and mechanical properties of refractory MoNbHfZrTi high-entropy alloy. Mater and Desi. 2015;81:87-94.
13. Maiti S, et al. Structural-disorder and its effect on mechanical properties in single-phase TaNbHfZr high-entropy alloy. Acta Mater. 2016;106:87-97.
14. Yao HW, et al. NbTaV-(Ti,W) refractory high-entropy alloys: Experiments and modeling. Mater Sci Eng A. 2016;674:203-211.
15. Praveen S, et al. Exceptional resistance to grain growth in nanocrystalline CoCrFeNi high entropy alloy at high homologous temperatures. Jour of Allo and Compo. 2016;662:361-367.
16. Aguilar C, et al. Fabrication of nanocrystalline alloys Cu-Cr-Mo super satured solid solution by mechanical alloying. Mater Chem and Phy. 2014;146:493-502.
17. Sharma AS, et al. High-entropy alloys and metallic nanocomposites: Processing challenges, microstructure development and property enhancement. Mater Scien and Engin R: Rep. 2018;131:1-42.
18. Koch CC. Nanocrystalline high-entropy alloys. J Mater Res. 2017;32:3435-3444.
19. Suryanarayana C, et al. The science and technology of mechanical alloying. Mater Sci Eng A. 2001;304-306:151-158.
20. Kang B, et al. Ultra-high strength WNbMoTaV high- entropy alloys with fine grain structure fabricated by powder metallurgical process. Mater Sci Eng A. 2018;712:616–624.

21. Cao Y, et al. Precipitation behavior and mechanical properties of a hot-worked TiNbTa0.5ZrAl0.5 refractory high entropy alloy. Inter Jour of Refr Met and Ha Mate. 2020;86.
22. Guo W, et al. Microstructures and mechanical properties of ductile NbTaTiV refractory high entropy alloy prepared by powder metallurgy. Jou of Alloand Comp. 2019;776:428-436.
23. Takeuchi A, et al. Classification of bulk metallic glasses by atomic size difference, heat of mixing and period of constituent elements and its application to characterization of the main alloying element. Mater Transac. 2005;46:2817-2829.
24. Chen YL, et al. Competition between elements during mechanical alloying in an octonary multi-principle-element alloy system. Jou of Allo and Comp. 2009;481:768-775.
25. Long Y, et al. Enhanced strength of a mechanical alloyed NbMoTaWVTi refractory high entropy alloy. Materials. 2018;11:1-8.
26. Oleszak D, et al. High entropy multicomponent WMoNbZrV alloy processed by mechanical alloying. Materials Lett. 2018;232:160-162.
27. Tong Y, et al. Different-shaped ultrafine MoNbTaW HEA powders prepared via mechanical alloying. Mater 2018;10:1-8.
28. Kumar A, et al. Mechanically alloyed high entropy alloys: Existing challenges and opportunities. J Mater Res and Technol. 2022;17:2431-2456.
29. Wang G, et al. Synthesis and thermal stability of a nanocrystalline MoNbTaTiV refractory high-entropy alloy via mechanical alloying. Inter Jour of Refra Met and Har Mater. 2019;84:104988.
30. Das S, et al. Mechanical alloying of W-Mo-V-Cr-Ta high entropy alloys. Mate Scie and Engin. 2018;346:1.
31. Xin SW, et al. Ultrahard bulk nanocrystalline VNbMoTaW high-entropy alloy. Jour of Allo and Compo. 2018;769:597-604.
32. Mizutani U. Hume-rothery rules for structurally complex alloys phases. CRC Press Taylor and Francis Group. 2011.
33. Guo S, et al. Effect of valence electron concentration on stability of fcc or bcc phase in high entropy alloys. Journal of Applied Physics. 2011;109:10.
34. Couzinié JP, et al. Comprehensive data compilation on the mechanical properties of refractory high-entropy alloys. Data in Brief. 2018;21:1622-1641.
35. Han ZD, et al. Microstructures and mechanical properties of TixNbMoTaW refractory high-entropy alloys. Mater Sci Eng A. 2017;712:380–385.
36. Xiao B, et al. Microstructure and mechanical properties of WMoTaNbTi refractory high-entropy alloys fabricated by selective electron beam melting. Jour of Materi Scien and Technol. 2022;108:54-63.
37. Vaidya M, et al. High-entropy alloys by mechanical alloying: A review. J Mater Res. 2019;34:664-686.
38. Guo S, et al. Phase stability in high entropy alloys: Formation of solid-solution phase or amorphous phase. Prog Nat Sci. 2011;21:433-446.
39. Gedevanishvili S, et al. The effect of ZrO_2 grinding media on the attrition milling of FeAl with Y_2O_3. Mater Sci Eng A. 2004;369:236-240.
40. De J, et al. Origin of contamination and role of mechanochemistry during mechanical alloying: the case of Ag-Te alloys. Mater Sci Eng A. 2007;448-451:1062-1066.